Cytoarchitecture of the Retinal Ganglion Cells in the Rat

John Danias, Fran Shen, David Goldblum, Bin Chen, Jerome Ramos-Esteban, Steven M. Podos, and Thom Mittag

Purpose. To determine the number and cytoarchitecture of retinal ganglion cells (RGCs) in the female Wistar rat, by using a newly devised procedure for rapid RGC counting in the entire retina that avoids assumptions about RGC spatial arrangement.

Methods. RGCs of normal female Wistar rats were retrogradely labeled with a fluorescent tracer. Automated counting was accomplished by applying standard imaging software to analysis of all labeled cells in retinal flatmounts. The method was validated by comparison of automated and manual counts of 70,000 RGCs in frames covering the density range in the normal rat retina of 600 to 3600 RGC/mm^2. RGC numbers were determined for each retina and compared with the contralateral retina of the same animal. RGC density maps were constructed for each retina. RGC size distribution was determined.

Results. Automated RGC counting showed a good linear correlation with manual counting ($R^2 = 0.9416$). Mean total RGC count in 10 rat eyes was 97,609 ± 3,930 (SEM) per eye. Contralateral eyes differed by an average of 4.1% (3983 ± 5098 RGCs). Size analysis calculated from cell areas confirmed that the majority of rat RGCs are between 7 and 21.5 μm in equivalent diameter. The RGC counts for all frames at the same eccentricity in all 10 of the retinas showed that variability increased with eccentricity and increased further as the fractional area of the retina sampled at each eccentricity was reduced. There was also significant variability in the spatial density of the RGCs at the same eccentricity location between different eyes. Comparison of total RGC counts between left and right eyes estimated from RGC counts in sectors of the retina (hemiretinas or quadrants) showed increased variability compared with counting all the RGCs in a retina.

Conclusions. RGCs in the Wistar rat display significant variability in their cytoarchitecture. Such variability can make quantification by sampling problematic for diffuse, and particularly, for focal RGC losses resulting from experimental interventions, unless virtually the entire RGC population is counted. (*Invest Ophthalmol Vis Sci.* 2002;43:587–594)

From the Department of Ophthalmology, Mt. Sinai School of Medicine, New York, New York.

Supported by National Eye Institute Grants K08 EY00390, EY01867, and EY11649; the Swiss National Foundation; M. & W. Lichtenstein-Stiftung; the Eye Bank for Sight Restoration Glaucoma Research and Training Fund; Research to Prevent Blindness; and the May and Samuel Rudin Foundation, Inc.

Submitted for publication June 5, 2001; revised September 10, 2001; accepted October 18, 2001.

Commercial relationships policy: P.

The publication costs of this article were defrayed in part by page charge payment. This article must therefore be marked "*advertisement*" in accordance with 18 U.S.C. §1734 solely to indicate this fact.

Corresponding author: John Danias, Department of Ophthalmology, Box 1183, Mt. Sinai School of Medicine, 1 Gustave L. Levy Place, New York, NY 10029; john.danias@mssm.edu.

Quantitation of retinal ganglion cell (RGCs) is a procedure that is often used to monitor the effects of noxious stimuli leading to cell death in the retina. This procedure has been applied to several experimental rodent retinal disease models, such as ischemia-reperfusion,[1] partial optic nerve crush,[2] optic nerve axotomy,[3,4] excitotoxin injection,[5] or chronic elevation of intraocular pressure (IOP).[6,7] The experimental eye is usually compared with the contralateral control eye for changes in the RGC number. Quantitation of RGC number has been performed by extrapolation from cell counts obtained from representative cross-sections, areas of retina in flatmounts, or by counting a proportion of the RGC axons in cross-sections of the optic nerve. Sampling methods are used in all these quantification procedures to overcome the difficulty of counting the large number of RGCs or their axons and the variations in cell or axon density. However, changes in the number of RGCs determined by comparison of sampled areas in retinal pairs has greatest reliability if it can be shown that the sampled areas from equivalent locations in the two retinas have equivalent RGC densities at the beginning of the experiment.

There is a general radial symmetry in the spatial distribution of RGCs in the rat eye, with decreasing RGC density progressing from the optic nerve head to the retinal periphery. This symmetry is often assumed to be 360°, with the RGC density equivalent at the same eccentricity along any radial meridian.[7] Although some early evidence of RGC spatial distribution determined in a few rodent retinas suggests that a strict radial symmetry may not be entirely correct,[8,9] the methods used in those studies have certain caveats. Identification of RGCs based on size criteria alone[8] cannot completely discriminate between RGCs and displaced amacrine cells, which can make up almost 50% of cells in the RGC layer in the rat.[10] Furthermore, retrograde labeling of the RGCs with large molecular weight markers, such as horseradish peroxidase (HRP),[9] is variable and depends on the degree of uptake and the location of application of the HRP in the brain.[11,12]

In an effort to establish the validity of the underlying assumptions when sampling is used to quantify RGCs by counting their cell bodies, we have developed a sampling-independent procedure that counts retrograde dye-labeled RGCs in flatmounts of the rat retina and provides information on the spatial geometry and relative size distribution of RGCs. This method relies on efficient retrograde labeling of RGCs, automated image acquisition from retinal flatmounts, and computerized analysis of the digitized images. It has potential application for RGC quantitation in any of the experimental animal models in which sampling methods of retrograde-labeled RGCs can be used (mouse, rat, cat, monkey).

Materials and Methods

Female Wistar rats weighing more than 180 g were used. All experiments adhered to the ARVO Statement for the Use of Animals in Ophthalmic and Vision Research. In the initial phases of this study, RGCs were retrogradely labeled by multiple stereotactic injections of a fluorescent tracer (Fluorogold; Fluorochrome, Inc., Denver CO) into the superior colliculus (SC) at various locations.[6,7] However, we found that labeling was not always consistent, with some areas of the retina

occasionally having labeling too weak for imaging by the digital camera setup used (data not shown). We thus used a method to label the SC over its entire surface.[13] This allowed us to consistently label RGCs over the entire retinal area with the fluorescent dye. Inspection under UV illumination of serial brain sections in the animals 1 week after the procedure revealed penetration of the dye throughout the whole extent of the SC (data not shown).

Under ketamine-acepromazine-xylazine anesthesia an opening was created in the skull approximately 6 mm posterior to Bregma, 1 mm on either side of the median raphe. The exposed occipital cortex was aspirated to expose the underlying superior colliculi. A pledget of absorbable gelatin (Gelfoam; Pharmacia & Upjohn, Kalamazoo, MI) soaked in 5% fluorescent tracer in sterile water was applied on the surface of the SC. Silicone grease was used to cover the gelatin and fill the skull opening and the skin was sutured after the incision was treated with topical antibiotic ointment and topical anesthetic. The animals were allowed to recover and were killed 7 days later.

Under the anesthesia described earlier, the animals were cardiac perfused with ice cold 4% paraformaldehyde in phosphate buffered saline (PBS). The eyes were enucleated, the anterior segments were removed, and the resultant eyecups were fixed in 4% paraformaldehyde for 2 hours at room temperature. One radial cut was created from the nasal margin of the retina for orientation using the caruncle as an orientation landmark. The retinas were then dissected from their attachment at the optic nerve using a trephine, and oriented on a microscope slide. Additional radial cuts were made to facilitate flattening of the retinas on the slide. Flat-mounted retinas were then air-dried to ensure flatness of the retina, coverslipped, and stored at 4°C in the dark until they were imaged.

Slides with flat-mounted retinas were observed on an epifluorescence microscope (Axiomat; Carl Zeiss, Inc., Thornwood, NY) equipped with a filter set (XF05; Omega Optical, Inc., Brattleboro, VT). The microscope had been modified to include a computer-driven motorized stage (Biopoint; Ludl Electronic Products, Ltd., Hawthorne NY), and a digital camera operating at ambient temperature (Pixera Corp., Los Gatos CA). Each retina was scanned in a raster pattern of adjacent nonoverlapping images with a ×10 objective (Fluar, NA 0.5; Zeiss). This low-power objective has sufficient depth of field to maintain focus of imaged RGCs in a frame despite the imperfect planarity in retinal flatmounts prepared as described. The resolution of each image was 0.92 pixels/μm^2. Each retina was completely imaged in 200 to 250 frames of 0.3335 mm^2 each, which took approximately 3 hours to accomplish. Frames had a space approximately 4 μm wide between them, so that approximately 1.5% of the total retinal area was not imaged. At this interframe spacing, cells not counted because of the watershedding algorithm that tends to remove the partially imaged cells at the frame edge, would be in the small size range of cells from 7 to 11.5 μm in diameter (described later). This size range represents approximately 30% of RGCs, and thus the error (number of cells not counted) caused by nonoverlapping frames is approximately 0.5%. Therefore, no attempt was made to correct for partial cells not counted at the edges of each frame. Overcounting caused by partially imaged cells at the edges of each frame represents a minimal error, because watershed segmentation tends to eliminate those cells that are mostly outside the frame but counts those cells that are mostly inside the frame. Although the error introduced by double counting of large cells or aggregates of small cells is expected to be minimal (<1%) because of the reasons just outlined, its magnitude has not been determined in this study. However, any errors introduced by either under- or overcounting of cells at edges are corrected by the use of the correction factor (described later). The total area of each retina was determined from the sum of retinal areas in the full and partial frames, as will be described.

Color (red-green-blue [RGB]) images obtained from the digital camera were saved for further analysis. Analysis was performed on computer, using commercially available software. The image processing was performed with image management software (Photoshop ver. 5.5; Adobe Systems, Inc., San Jose CA). After the RGB images were converted to gray scale, a high-pass filter was used to eliminate camera noise and background fluorescence from the nerve fiber layer (NFL). The image was subsequently intensity thresholded (threshold 128) and inverted so that fluorescent cells would appear as black objects on a white background. Euclidian distance map (EDM) erosion[14] followed by watershed segmentation[14] was applied to maximize resolution of touching cells. Figure 1 illustrates the transformation applied to the RGB image of a representative frame to use automated quantification.

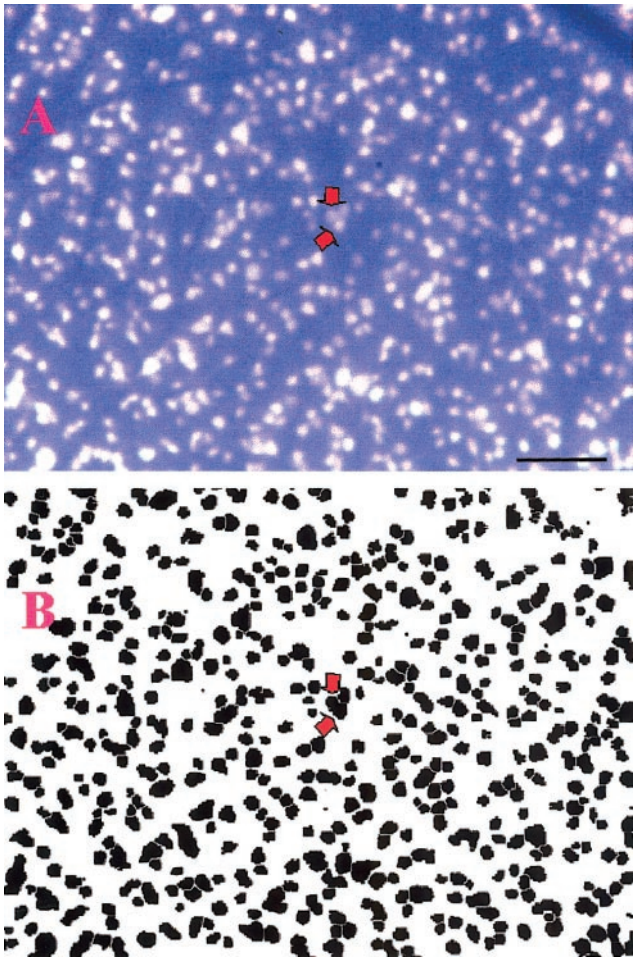

Figure 1. Representative RGB image (RGC density, approximately 1800 RGCs/mm^2) from a flatmounted normal rat retina and corresponding binary image used for automated RGC counting. Note the relatively good size correspondence of RGCs in the RGB and binary images. *Arrow*: cluster of cells that would not be discriminated as individual cells by the conversion algorithm. This limitation of automated counting (which results in undercounts for frames at higher cell densities) is compensated for by using a correction factor for the cell densities. Scale bar, 100 μm.

Rapid counting of retinal ganglion cells in the processed binary images was achieved with image analysis software (Image-Tool, ver. 2.0; University of Texas Health Sciences Center San Antonio [UTHSCSA], San Antonio, TX), using a size threshold of 31 pixels for the image magnification set-up described earlier. This size threshold was estimated from published data on RGC size, directly by visual inspection of the smallest RGC in the unprocessed images, and specifically determined by size analysis of the objects in the binary images of all 10 retinas (see the Results section). Once automated, the whole process of object counting was performed on the RGB images as a stack without any operator input and could be accomplished in less than 2 hours for each retina.

Cell density was calculated for each frame by dividing the number of objects in each frame by the area occupied by retinal tissue in the frame (in nonfull frames this area was easily measured by thresholding the image in the RGB channels). The object density was then con-

verted to cell density by applying a correction, as described later. After cell density was calculated for each frame, the image management and image analysis software programs (Photoshop; Adobe, and Image-Tool, respectively) were used to generate color-coded maps of cell density for each retina.

The algorithm used for converting the RGB into binary images suitable for automated counting was validated by performing manual counts on 12 to 15 unprocessed full RGB frames from each retina. Frames to be counted manually were selected at random and covered high-, medium-, and low-density areas without respect to location. Manual counting of frames was performed using the "count-and-tag" routine of Image-Tool. Unbiased counting rules were used for counting edge-touching cells.[15,16] Manually counted frames covering the full range of RGC densities were then compared with the corresponding automated object counts obtained for the same frame after image processing, as has been described.

Morphologic size data based on the area of the counted objects was obtained for all frames using the image management program (Photoshop; Adobe), and were analyzed using a data management program (Excel 2000; Microsoft Corp, Redmond, WA). Statistical analysis was performed on computer (NCSS statistical analysis software, Kaysville, UT).

Results

Imaging

Figure 1 shows a representative frame of imaged RGCs in RGB mode and its corresponding binary image. An example of an aggregate of cells not individually resolved is marked (Fig. 1A, arrow). This limitation of automated counting (which results in undercounts for frames at higher cell densities) is compensated for by using a correction factor for the cell densities, as described in the following section.

Method Validation

The object-size threshold corresponding to the smallest RGC was determined by plotting the object areas (in pixels) against the number of objects for all 10 retinas (Fig. 2). Objects less than 25 pixels in size include background and some small partial images, whereas objects 30 pixels in size correspond to the smallest cell size, approximately 7 μm in diameter (indicated by the arrow-marked inflection point in the plots).

Twelve to 15 nonadjacent frames from each retina (127 frames in all) with densities ranging from 600 to 3600 cells/mm^2 (a total of 70,186 retrogradely labeled cells) were used for the comparison of automated counts with manual counts of labeled RGCs. Manual counts of visually identified

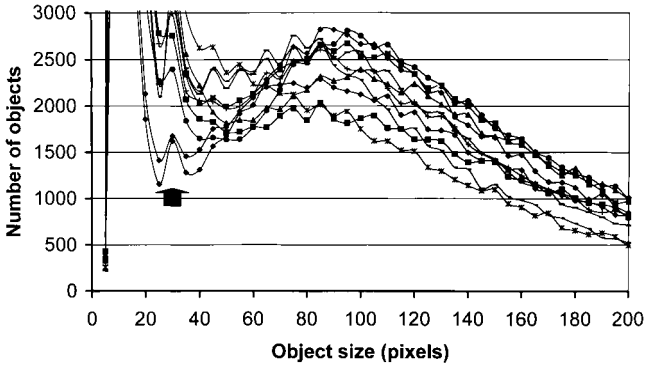

Figure 2. Size analysis of objects in binary images. Each line represents one retina. The histogram covers the range of objects between 0 and 200 pixels in size. High abundance background (<15 pixels in size) and objects larger than 200 pixels are off the graph. *Arrow*: area of smallest cell and size threshold used for automated counting.

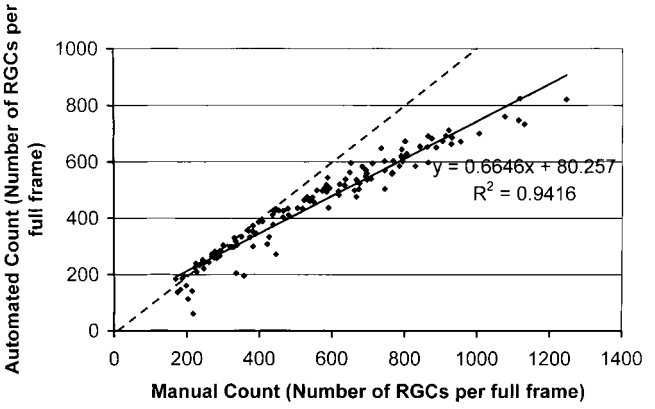

Figure 3. Manual versus automated counting of RGCs of 127 full frames of 0.33 mm^2 each, selected from 10 retinas and covering the full density range in the rat retina. Best-fit linear regression equation and corresponding correlation coefficient (R^2) are indicated. Broken line indicates 1-to-1 correlation—that is, manual counts equal automated counts.

RGCs were performed by two of the authors (JD, FS) who were masked as to the count obtained from the automated analysis.

For counts of frames in individual retinas and for all the frames from 10 retinas, there was a strong correlation between the two counting methods (Fig. 3). A good fit to the data are obtained with either a logarithmic curve ($y = 0.1907\ln(x) + 0.3463$, $R^2 = 0.9445$) or a linear equation with $R^2 = 0.9416$, shown in Figure 3. The linear fit was best described by the equation (automated counts) = (manual count) $\times$ 0.6646 + 80.257. Because all frames counted manually were full frames (frames with partial retinal area at the edges or at the cuts of the flatmount were excluded in this analysis), the same equation holds for the relationship between the cell densities in these frames (i.e., automated density = manual density $\times$ 0.6646 + 80.257/frame area). The above equation was used to correct the density of RGCs in each frame determined by automated counting to approximate the true number of RGCs present if the frame had been counted manually (the linear correlation was preferred to the logarithmic because of the ease of calculations). Because this correction factor was derived from a pool of frames from all retinas studied (rather than a separate correction factor for each retina) it was unclear whether it applied equally well to all retinas, and all the further analyses and comparisons of counts in the sections that follow were therefore also performed on the raw automated counts (i.e., without correction). Although total numbers were lower (because of the increasing systematic undercount with density by the automated method), the conclusions were not significantly different from those obtained using the corrected data, which are presented herein.

RGC Count and Density

RGC counts for the five pairs of retinas studied are summarized in Figure 4. The data are presented as densities (total number of RGCs/total retinal area) to correct for the small variations in retinal area of flatmounts prepared from different eyes. Mean RGC count for all 10 retinas was 97,609 $\pm$ 3,930 (SEM) per retina. Mean RGC counts for left and right eyes were 95,618 $\pm$ 5,512 and 99,600 $\pm$ 6,087, respectively. The average difference between pairs of retinas from the same animal was 3983 $\pm$ 5098 RGCs ($P = 0.48$ paired t-test, not significantly different). However, average RGC densities for both eyes varied significantly ($P = 0.005$, ANOVA) between different animals (Fig. 4), whereas RGC count differences between animals

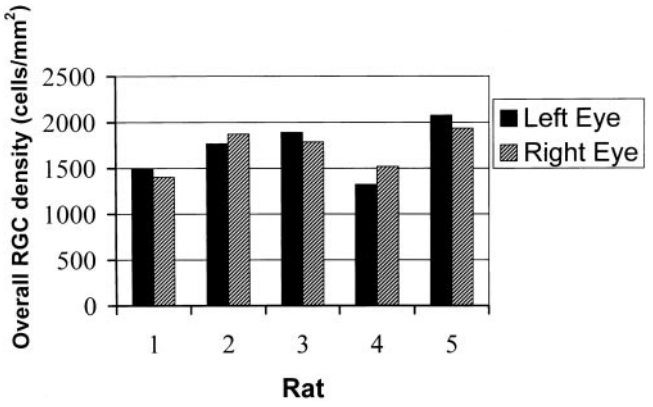

FIGURE 4. Overall RGC density per retina in normal adult female Wistar rats. The RGC density calculated by total RGC number/total retinal area is plotted for pairs of eyes.

did not quite reach the 95% level of statistical significance ($P = 0.06$, ANOVA). Area per retina for the 10 eyes averaged was 57.54 ± 1.56 mm^2. Retinal area did not differ significantly between animals ($P = 0.1$, ANOVA), nor between left and right eyes ($P = 0.42$ paired *t*-test, not significantly different).

Spatial Maps and Locational Variation of RGC Density

To determine the cytoarchitecture of RGCs over the entire retina, color-coded RGC density maps were assembled from all the frames used to image each of the 10 retinas (Fig. 5). Inspection of these maps provided direct evidence of a general decrease of the RGC density with increasing distance from the optic nerve head. A plot of RGC density against eccentricity (Fig. 6) showed that the highest density locus extended outward to 2.3 mm from the optic nerve (no difference in density between points up to 2.3 mm, Bonferroni multiple comparisons, $\alpha = 0.05$). The density variations for the 10 retinas shown in Figure 6 and their density maps (Fig. 5) indicates that the RGC density distribution varied substantially between retinas. The highest density areas are not always at the same location in the retina. Additionally, the RGC density did not have a high degree of uniformity at the same eccentric distance on all radial meridians. This finding is quantitatively indicated by the SDs of the means of densities at different eccentricities shown in Figure 6.

Sector Analysis of Hemiretinas or Quadrants

Comparison of the number of RGCs in the superior, inferior, nasal, or temporal half of each retina for the 10 retinas revealed

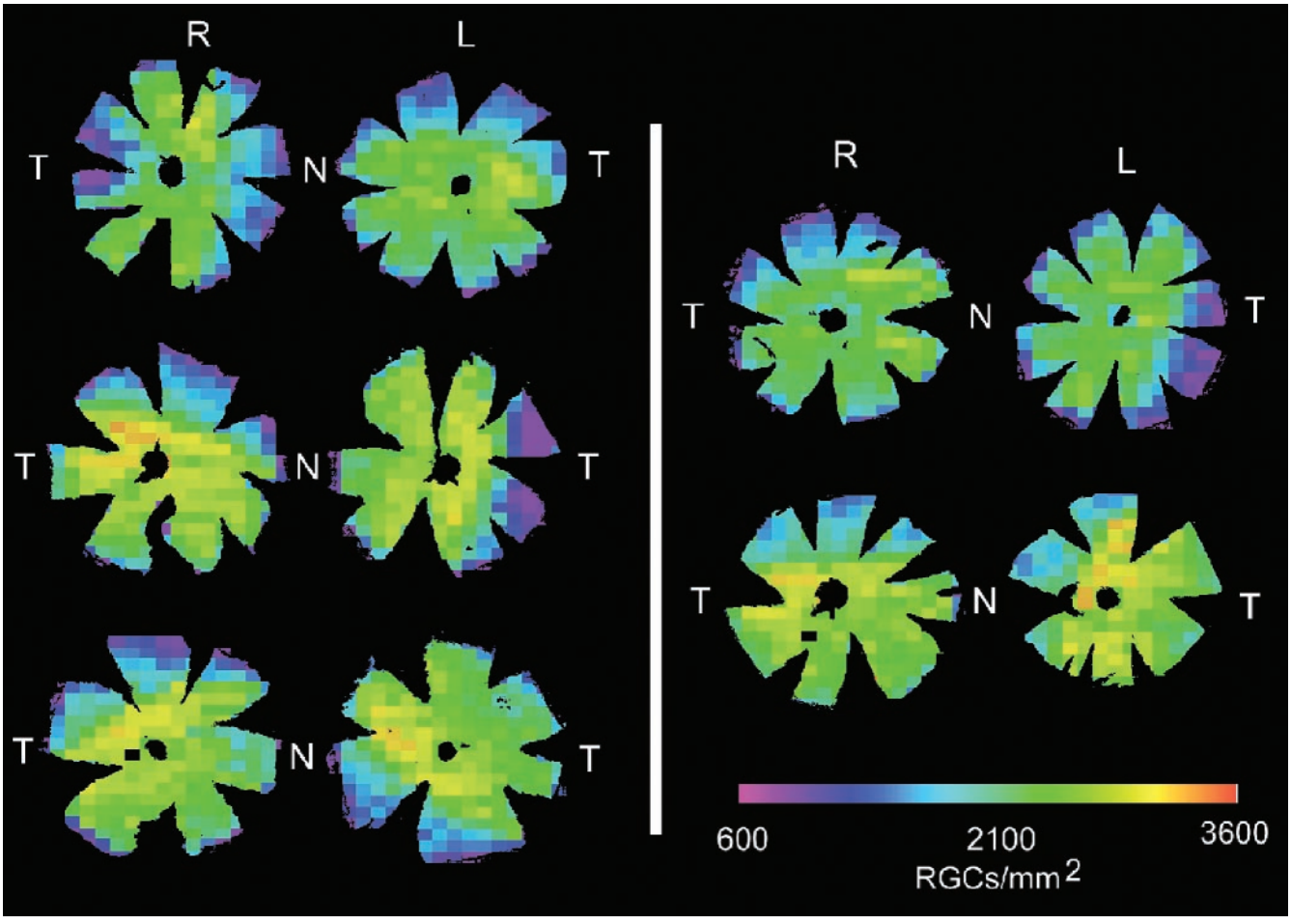

FIGURE 5. Pseudocolor maps of RGC density in the five pairs of rat eyes. Retinas are oriented superior retina up and nasal hemiretinas adjacent. Color scale ranges from a minimum of 600 RGC/mm^2 to a maximum of 3600 RGC/mm^2. Black frames in two retinas correspond to missing data. Note that the area of highest density does not localize consistently in the same retinal quadrant. T, temporal; N, nasal; R, right eye; L, left eye.

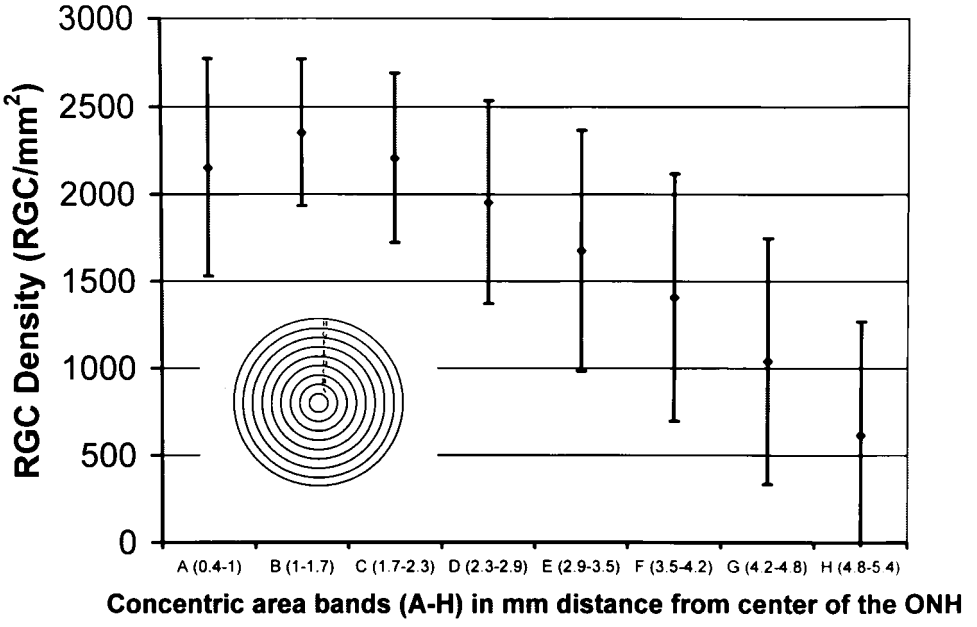

FIGURE 6. RGC density (±SD) in area bands at various eccentricities from the ONH. Eccentricities are indicated at the central point of eight concentric bands of equal width (0.6 mm) dividing the distance from the optic nerve head to the edge of the peripheral retina, labeled A–H.

no significant difference ($P = 0.41$ and $P = 0.11$, paired *t*-test, respectively) although in 8 of 10 eyes the nasal hemiretina had more cells (Fig. 7A) There was also no significant difference between contralateral eyes in RGC count in the corresponding hemiretina (Fig. 7B). These findings were the same when correction was made for small differences in the total area of each hemiretina. Similar analysis of quadrants (Figs. 7C, 7D) also revealed no significant differences between the number of RGCs present in the various quadrants between eyes ($P = 0.24$ ANOVA) and between pairs of eyes ($P = 0.48$, paired *t*-test) after correction for the total area of each quadrant.

Size Analysis

Size analysis (apparent cell diameter based on area) was performed using the same binary images that were used to count RGCs. Binary images superimposed on the color RGB images (pairs similar to the one shown in Figure 1) established that, for individual cells over the size range, RGB and binary images were very close in size, with binary images approximately 15% smaller (data not shown). The corrected size analysis is shown in Figure 8 where the equivalent diameter calculated from cell areas (assuming a circular object) was used to categorize the objects imaged. Approximately 95% of the objects corre-

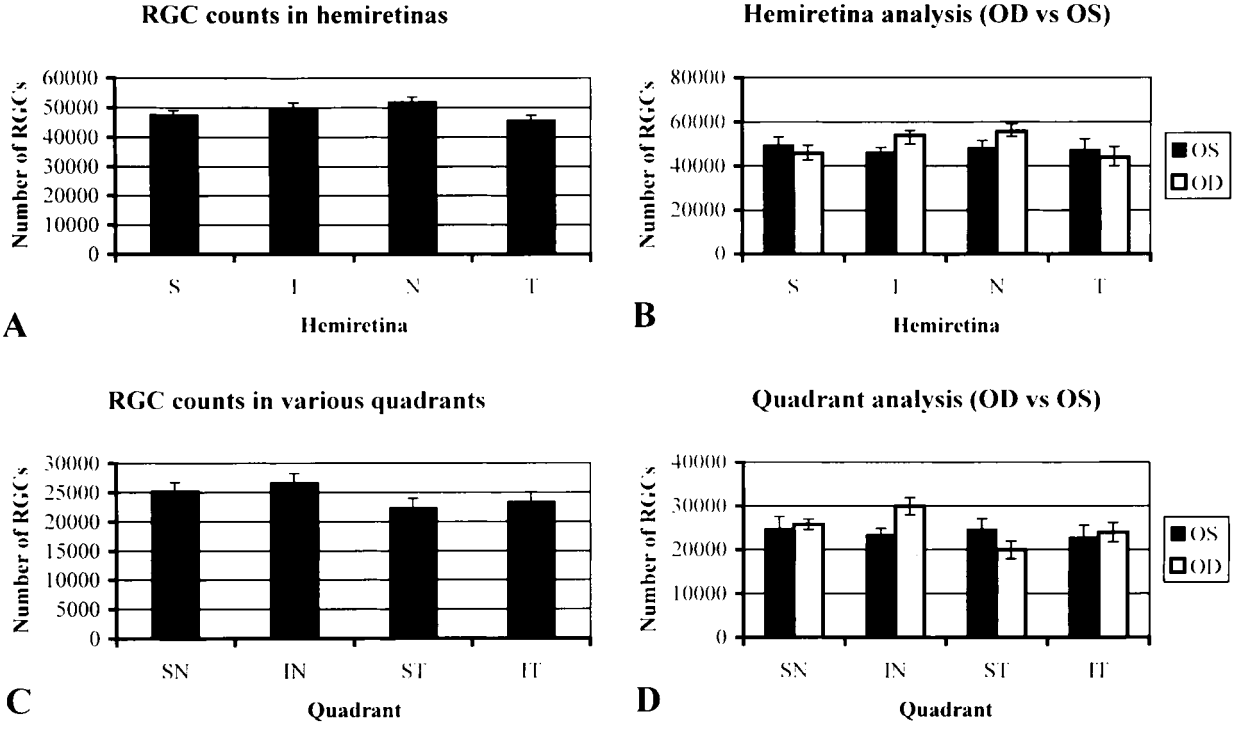

FIGURE 7. Sector analysis of RGC counts in hemiretinas (**A**, **B**) and quadrants (**C**, **D**) in all, $n = 10$ (**A**, **C**) and contralateral (**B**, **D**), $n = 5$ eyes. S, superior; I, inferior; N, nasal; T, temporal; SN, superonasal; IN, inferonasal; ST, superotemporal; IT, inferotemporal.

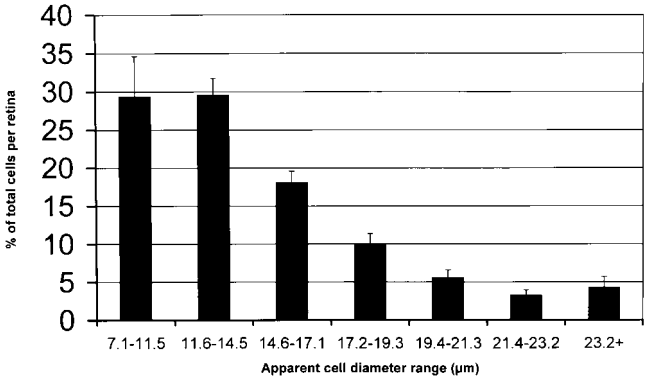

FIGURE 8. Size distribution of counted objects as a function of the apparent cell diameter. Cell diameter was calculated for a circular cell of equivalent area after correcting for the approximately 15% difference between the cell size in color RGB images and object size in binary images.

sponded to RGCs with an equivalent diameter between 7.1 and 21.4 μm, in good agreement with the data of Perry[17] for the range and largest size of RGCs in the rat retina. Objects with diameters larger than this size probably represent aggregates of cells too close to be discriminated by the counting algorithm.

Error Estimation in Determining RGC Density for Various Eccentricity Sampling Levels

To determine the effect of eccentricity sampling of retinal areas without regard to the angular position within the retina, we systematically thinned the data for the 10 retinas by examining the RGC count in every second (50%), fourth (25%), and sixth frame (16.67%) in eight concentric bands from the ONH to the retinal edge. The SEM density for each area band is plotted as a function of distance from the center of the ONH in Figure 9. As expected, the error in RGC density estimation at each eccentricity increased as the fractional area sampled was reduced. Additionally, the plots are U-shaped, indicating that there is less uniformity of RGC density at locations near the ONH and at the outer edge of the retinas compared with the areas between.

DISCUSSION

Retinal ganglion cytoarchitecture has been studied most thoroughly in humans and primates.[18,19] Despite the significance of rodents in research, cytoarchitecture of the RGCs in the rat over the entire retina is less well characterized. Studies on the rat were reported in 1932,[20] in 1977,[8] and in the 1980s.[9,21] The first two studies were performed with nonspecific general histologic stains and differentiated RGCs by size criteria alone. It is possible that these measurements were inaccurate, because of the large number of displaced amacrine cells present in the RGC layer of the rat retina, which can comprise up to 50% of the total cells in areas of the RGC layer.[17] The most recent studies used retrograde labeling of RGCs with HRP, injected stereotactically into the SC. Although retrograde labeling with HRP avoids some of the problems of earlier studies, it introduces other potential pitfalls. In particular, it has been shown that HRP labeling is variable,[11] often dependent on the amount of tissue destruction at the site of injection, with more

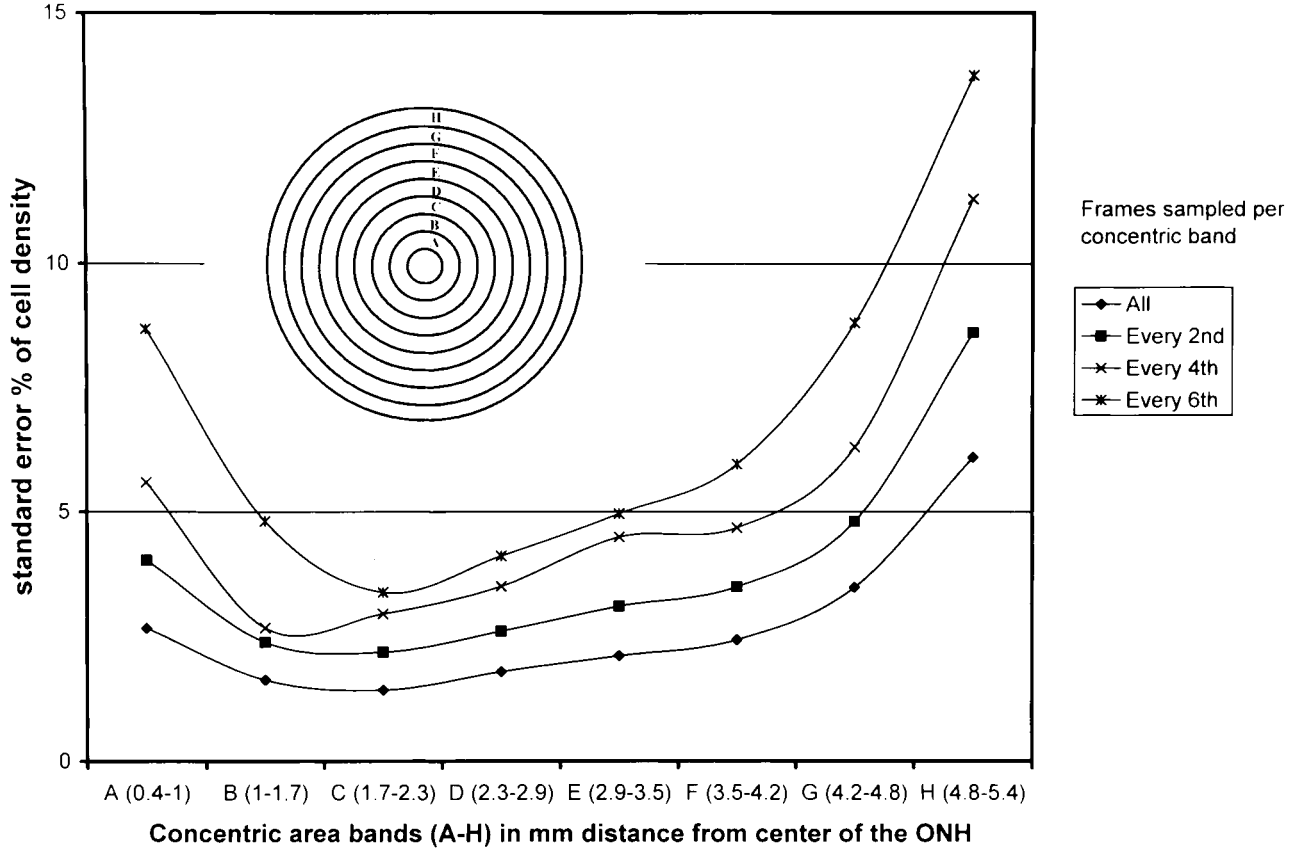

FIGURE 9. Percentage SEM of cell density (RGC/mm^2) as a function of eccentricity determined for various degrees of sampling of frames in eight concentric area bands labeled A–H. Note that uniformity of RGC density decreases at the periphery (5 mm) and near the ONH (0.7 mm), compared with areas between.

destruction resulting in better labeling.[12] In the initial phases of our study we confirmed the difficulty of consistently obtaining a completely labeled RGC population in retinas by SC injection, even when using more water-soluble tracer molecules smaller in size and with better uptake than HRP.

Despite a lack of accurate information on rat RGC cytoarchitecture, rats are most often used as a model for conditions that affect RGCs such as metabolic and toxic retinopathies and glaucoma. Such investigations use estimated total RGC counts or density obtained by sampling methods as an endpoint for experimental interventions. The sampling methods and the number of animals to be used in an experiment are based on several apparently reasonable assumptions that have not been rigorously examined for their validity: (1) that the eyes of rodents of the same strain have equivalent numbers of RGCs; (2) that the two eyes of an individual animal have the same number of RGCs; (3) that the retina is radially symmetric so that RGC density is equivalent at points the same distance from the optic nerve on any radial meridian; and (4) that the effect of the experimental intervention is homogeneous throughout the retina.

These assumptions are used to justify a sampling strategy to estimate total RGCs by determining the density at points over 360° at various eccentricities from the optic nerve head, thus allowing comparisons between experimental groups with a reasonable number of animals. Because the most tedious part of this strategy is counting the RGCs, either directly at the microscope or from still frames, the number of animals used in such experiments was usually less than 10, and the number of RGCs counted was 3% to 4%[7] or 6% to 10%,[10,21,22] but maximally only approximately 15% of the total.[6,8]

Counting of the ON axons is an alternative way to quantitate RGCs. However, this procedure also relies on sampling, usually less than 20% of axons being counted. In addition, nonmyelinated axons are difficult to determine. Furthermore, ON axon counting is not as amenable to automated counting as are the more widely spaced RGC somata in a retinal flatmount. In addition, ON axons do not provide reliable size information on the RGC cell bodies, which appears to change in some pathologic conditions.

To determine the limits of the first three of the listed assumptions, we investigated the spatial distribution of RGCs in five normal young female Wistar rats by counting almost all the RGCs in each of the 10 eyes. Our results obtained using an automated method indicate that there are significant variabilities associated with some of the assumptions.

Amidine dyes used for automated counting of retrogradely labeled RGCs have properties that are especially useful for this purpose. The highly water-soluble dicationic amidine dye (Fluorogold) used in this study readily penetrates the SC from a surface application. This avoids the damage to the termini of RGC axons that occurs when dyes are applied by multiple injections into the SC. The dye is well taken up by RGC axon nerve terminals and transported to the cell bodies, where it is retained without significant leakage for up to 2 weeks. The accumulation of the dye in ganglion cell bodies over 7 days after application is particularly important for automated counting, because the fluorescence of the RGC soma is very much greater than that due to the amount of dye in transit in the retinal NFL. As shown in Figure 1, the dye in the NFL was insufficient to image the nerve fiber bundles, and this dye in the NFL contributes to background and does not affect the ability to image and quantify RGCs. The consistency of RGC counts in the whole retina, hemiretinas, and quadrants in contralateral eyes shows that incomplete uptake and/or transport of the dye used to label RGCs is unlikely when using the particular fluorescent dye (Fluorogold), as described herein.

In the rat a small minority of RGCs (5%–10%) do not project to the SC[9,23,24] and thus were not counted in our study. After adjusting for these uncounted RGCs we estimate that the true total RGC count is between 102,746 and 107,370 ± 4,143 (SEM) in the adult female Wistar rat retina, which is in good agreement with published independent estimates of rat optic nerve axon counts ranging from 96,200 to 118,300.[25,26] However, the total RGC count appears to vary considerably among individuals of the same strain as shown in Figure 4. This may be because Wistar is an outbred rat strain, and the variability between different animals may be smaller in inbred strains. Although the two eyes of each animal have reasonably similar RGC numbers, the RGCs are not spatially arranged in an equivalent radially symmetric manner (Fig. 5).

The retinal density maps generated from counting almost all RGCs confirm that the rat does not have a visual streak, as is present in other animals, including humans. In addition, there was the unexpected finding that the highest RGC density did not appear to consistently localize in any one quadrant. This finding is in contrast to the results of Fukuda[8] and the observations of Lashley,[20] who reported that the highest RGC density is in the superotemporal quadrant. Our findings also do not coincide with the results of Dreher et al.,[9] and McCall et al.,[21] who present isodensity maps of the rat retina that localize the area of maximum RGC density either superotemporally,[9] or temporally[21] and the area of minimum RGC density superiorly.[21] Because the methods used in these earlier studies have drawbacks, as discussed earlier, it is possible that these RGC density maps are unreliable. Among the eyes that we studied, maximal RGC localization in the temporal-superotemporal quadrant was present or suggested in only 6 of 10 eyes. Such variability is not unprecedented, however. Even in species with more complex retinas that rely more on good visual ability than the albino rat (including the human), regional density differences among eyes can range up to 40%, although such variability is significantly smaller when comparing the two eyes of one individual.[19] Consequently, the nerve fiber layer architecture also does not maintain strict retinotopy.[27]

The present method used to count RGCs is novel, but uses generally available hardware and software for image analysis. The excellent, almost linear, correlation between manual and automated counts indicates that the algorithm is very robust in the range of densities found on the images analyzed. The increasing systematic undercount with density by the automated method does not affect the validity of conclusions based on comparisons of RGC numbers and densities. However, cell size analysis introduces a small systematic bias toward larger cells, because very small cells close to each other that are not resolved could be counted as one larger cell. Nevertheless, the ability to determine apparent cell-size distribution (Fig. 8) can be an important component of the automated counting method, in that changes in cell size have been reported in pathologic retinas[28] and differential vulnerability of size categories of RGCs has been proposed for certain pathologic conditions.[29]

It is evident from our data that results of sector-sampling comparisons of a significant fraction of the retinal area, such as quadrants or hemiretinas (i.e., 25% or 50% of the area of two contralateral retinas), can vary considerably (Fig. 7), thus making detection of small differences in RGC number more difficult than if the entire retina was counted. Even when the total number of RGCs is compared in two normal contralateral retinas, the difference can be up to 8%, making changes in the number of RGCs due to pathologic loss in the range up to 15% difficult to determine reliably. We have also determined for all 10 retinal flatmounts, the effect of different levels of eccentricity sampling in nested 0.6 mm wide concentric bands from the ONH out to the retinal edge (Fig. 9). The SEM increases as sampling level decreases from every second (50%) to every sixth (16.6%) frame in these concentric bands and also increases for any sampling level at the periphery and near the

ONH. A significant increase in SE of RGC density also occurs at the periphery when all the frames are counted. This finding indicates that cell density is much less uniform at the periphery than it is in the more central regions of the rat retina extending to within 1.5 mm of the ONH.

To summarize our findings, the total number of RGCs is fairly consistent in the two contralateral eyes of the Wistar rat. The rat retina does not exhibit strict radial symmetry, and the location of highest RGC density area is apparently random. Sampling of areas comprising 50% or 25% of the retinal area introduces a significant increase in variability that may obscure differences of up to 15% in RGC counts between paired retinas, caused by experimental interventions. To document such relatively small differences by counting RGCs in 50% or 25% of the retinal area (using the hemiretina or quadrant count data in Fig. 7), would require an increase in the number of eyes needed for analysis compared with when total counts are used. For example, the number of animals required would increase from 7 to 11 to 19 for detecting a 20% difference between control and experimental eyes ($P < 0.05$, power = 0.8, mean total RGC count for normal retina = 96,000) when total, hemiretinal, or quadrant counts are used, respectively. The presently described automated method for counting total RGCs improves the ability to detect differences and takes into account both uniform and focal loss of RGCs in experimental models. In addition, this method can be readily adapted to different imaging setups and for counting RGC densities in other species where retrograde labeling of RGCs with amidine dyes is feasible.

References

1. Lam T, Siew E, Chu R, Tso MO. Ameliorative effect of MK-801 on retinal ischemia. *J Ocul Pharmacol Ther.* 1997;13:129–137.
2. Yoles E, Wheeler LA, Schwartz M. Alpha-2-adrenoreceptor agonists are neuroprotective in a rat model of optic nerve degeneration. *Invest Ophthalmol Vis Sci.* 1999;40:65–73.
3. Villegas-Perez M, Vidal-Sanz M, Bray GM, Aguayo AJ. Influences of peripheral nerve grafts on the survival and regrowth of axotomized retinal ganglion cells in adult rats. *J Neurosci.* 1988;8:265–280.
4. Heiduschka P, Thanos S. Aurintricarboxylic acid promotes survival and regeneration of axotomised retinal ganglion cells in vivo. *Neuropharmacology.* 2000;39:889–902.
5. Vorwerk CK, Lipton SA, Zurakowski D, Hyman BT, Sabel BA, Dreyer EB. Chronic low-dose glutamate is toxic to retinal ganglion cells: toxicity blocked by memantine. *Invest Ophthalmol Vis Sci.* 1996;37:1618–1624.
6. Sawada A, Neufeld AH. Confirmation of the rat model of chronic. moderately elevated intraocular pressure. *Exp Eye Res.* 1999;69: 525–531.
7. Laquis S, Chaudhary P, Sharma SC. The patterns of retinal ganglion cell death in hypertensive eyes. *Brain Res.* 1998;784:100–104.
8. Fukuda Y. A three group classification of rat retinal ganglion cells: histological and physiological studies. *Brain Res*. 1977;119:327–344.
9. Dreher B, Sefton AJ, Ni SY, Nisbett G. The morphology, number, distribution and central projections of class I retinal ganglion cells in albino and hooded rats. *Brain Behav Evol.* 1985;26:10–48.
10. Perry V, Henderson Z, Linden R. Postnatal changes in retinal ganglion cell and optic axon populations in the pigmented rat. *J Comp Neurol.* 1983;219:356–368.
11. Bunt A, Lund RD, Lund JS. Retrograde axonal transport of horseradish peroxidase in ganglion cells of the albino rat retina. *Brain Res.* 1974;73:215–228.
12. Drager U, Olsen JF. Origins of crossed and uncrossed projections in pigmented and albino mice. *J Comp Neurol.* 1980;191:383–412.
13. Thanos S. Combined methods of retrograde staining: layer-separation and viscoelastic cell stabilization to isolate retinal ganglion cells in adult rats. *J Neurosci Methods.* 1998;83:113–24.
14. Russ JC. *The Image Analysis Handbook.* 3rd Ed., Boca Raton FL: CRC Press; 1998.
15. Mohand-Said S, Deudon-Combe A, Hicks D, et al. Normal retina releases a diffusible factor stimulating cone survival in the retinal degeneration mouse. *Proc Natl Acad Sci USA.* 1998;95:8357–8362.
16. Gundersen H, Bendtsen TF, Korbo L, et al. Some new, simple and efficient stereological methods and their use in pathological research and diagnosis. *Acta Pathol Microbiol Immunol Scand.* 1988;96:857–881.
17. Perry V. Evidence for an amacrine cell system in the ganglion cell layer of the rat retina. *Neuroscience.* 1981;6:931–944.
18. Stone J, Johnston E. The topography of primate retina: a study of the human, bushbaby, and new- and old-world monkeys. *J Comp Neurol.* 1981;196:205–223.
19. Curcio C, Allen KA. Topography of ganglion cells in human retina. *J Comp Neurol.* 1990;300:5–25.
20. Lashley K. The mechanism of vision V: the structure and image-forming power of the rat's eye. *J Comp Psychol.* 1932;13:173-200.
21. McCall M, Robinson SR, Dreher B. Differential retinal growth appears to be the primary factor producing the ganglion cell density gradient in the rat. *Neurosci Lett.* 1987;79:78–84.
22. Harvey AR, Robertson D. Time-course and extent of retinal ganglion cell death following ablation of the superior colliculus in neonatal rats. *J Comp Neurol.* 1992;325:83–94.
23. Cowey A, Perry VH. The projection of the temporal retina in rats studied by retrograde transport of horseradish peroxidase. *Exp Brain Res.* 1979;35:443–455.
24. Jeffery G. Retinal ganglion cell death and terminal field retraction in the developing rodent visual system. *Dev Brain Res.* 1984;13: 81–96.
25. Forrester J, Peters A. Nerve fibers in optic nerve of rat. *Nature.* 1967;214:245–247.
26. De-Juan J, Iniguez C, Carreres J. Number diameter and distribution of the rat optic nerve fibers. *Acta Anal* (*Basel*). 1978;102:294–299.
27. Fitzgibbon T, Taylor SF. Retinotopy of the human retinal nerve fibre layer and optic nerve head. *J Comp Neurol.* 1996;375:238–251.
28. Morgan J, Uchida H, Caprioli J. Retinal ganglion cell death in experimental glaucoma. *Br J Ophthalmol.* 2000;84:303–310.
29. Glovinsky Y, Quigley HA, Dunkelberger GR. Retinal ganglion cell loss is size dependent in experimental glaucoma. *Invest Ophthalmol Vis Sci.* 1991;32:484–491.